Simulation of Merging Neutron Stars in Full General Relativity

Masaru Shibata

Department of Earth and Space Science, Osaka University, Toyonaka, Japan
and
Graduate School of Arts and Sciences, University of Tokyo,
Komaba, Meguro, Japan[*]

Lecture given at the
Conference on Gravitational Waves:
Challenge to Theoretical Astrophysics
Trieste, 5-9 June 2000

LNS013009

[*]Present address. shibata@chianti.c.u-tokyo.ac.jp

Abstract

We have performed 3D numerical simulations for merger of equal mass binary neutron stars in full general relativity. We adopt a Γ-law equation of state in the form $P = (\Gamma - 1)\rho\varepsilon$ where P, ρ, ε and Γ are the pressure, rest mass density, specific internal energy, and the adiabatic constant. As initial conditions, we adopt models of irrotational binary neutron stars in a quasiequilibrium state. Simulations have been carried out for a wide range of Γ and compactness of neutron stars, paying particular attention to the final product and gravitational waves. We find that the final product depends sensitively on the initial compactness of the neutron stars: In a merger between sufficiently compact neutron stars, a black hole is formed in a dynamical timescale. As the compactness is decreased, the formation timescale becomes longer and longer. It is also found that a differentially rotating massive neutron star is formed instead of a black hole for less compact binary cases. In the case of black hole formation, the disk mass around the black hole appears to be very small; less than 1% of the total rest mass. It is indicated that waveforms of high-frequency gravitational waves after merger depend strongly on the compactness of neutron stars before the merger. We point out importance of detecting such gravitational waves of high frequency to constrain the maximum allowed mass of neutron stars.

1 Introduction

Interest in the final coalescing phase of binary neutron stars has been stimulated by the prospect of future observation of extragalactic, close binary neutron stars by gravitational wave detectors [1]. A statistical study indicates that mergers of binary neutron stars may occur at a few events per year within a distance of a few hundred Mpc [2]. Since the amplitude of gravitational waves from a binary of mass $\sim 3M_\odot$ (where $M_\odot$ denotes the solar mass) at a distance of ~ 100Mpc can be as large as $\sim 10^{-21}$, merger of binaries can be a promising source of gravitational waves for gravitational waves detectors. Although the frequency of gravitational waves in the merging regime will be larger than 1kHz (see Sec. 3) and lies beyond the upper end of the frequency range accessible to laser interferometers such as LIGO and VIRGO for a typical event at a distance about a few hundred Mpc, it may be observed using specially designed narrow band interferometers or resonant-mass detectors [1]. Such future observations, although it may not be achieved in near future, will provide valuable information about the merger mechanism of binary neutron stars and the final products.

Interest has also been stimulated by a hypothesis about the central engine of γ-ray bursts (GRBs) [3]. Recently, some of GRBs have been shown to be of cosmological origin [4]. In cosmological GRBs, the central sources must supply a large amount of the energy $\geq 10^{50}$ ergs in a very short timescale of order from a millisecond to a second. It has been suggested that the merger of binary neutron stars is a likely candidate for the powerful central source [3]. In the typical hypothetical scenario, the final product should be a system composed of a rotating black hole surrounded by a massive disk of mass $> 0.1M_\odot$, which could supply the large amount of energy by neutrino processes or by extracting the rotational energy of the black hole.

To investigate merger of binary neutron stars theoretically, numerical simulation appears to be the unique promising approach. Considerable effort has been made for this in the framework of Newtonian and post-Newtonian gravity (see, e.g., [5] for review and references). Although these simulations have clarified a wide variety of physical features which are important during the merger of binary neutron stars, a fully general relativistic (GR) treatment is obviously necessary for determining the final product and associated gravitational waves because GR effects are crucial.

Intense effort has been made for constructing a reliable code for 3D hydrodynamic simulation in full general relativity in the past decade (see, e.g., [6, 7, 8] for review and references). Recently, the author has succeeded in constructing a numerical code by which stable and fairly accurate simulations are feasible [8], and subsequently, he and collaborators have been performing fully GR, hydrodynamic simulations for a wide variety of astrophysical problems [8, 9, 10, 11, 12] including merging binary neutron stars. In this manuscript, we describe our method for numerical relativistic simulation and present some results with regard to merger of binary neutron stars.

The paper is organized as follows. In Sec. 2, we describe our formulation in 3D

numerical relativity. In Sec. 3, numerical results with regard to merger of binary neutron stars are presented, paying particular attention to the final product and gravitational waves. Sec. 4 is devoted to a summary. Throughout this paper, we adopt the units $G = c = 1$ where G and c denote the gravitational constant and speed of light, respectively. Latin and Greek indices denote spatial components ($1-3$) and space-time components ($0-3$), respectively. $\delta_{ij} (= \delta^{ij})$ denotes the Kronecker delta. We use Cartesian coordinates $x^k = (x, y, z)$ as the spatial coordinates; t denotes coordinate time.

2 Formulation

2.1 Basic equations

Numerical simulation is carried out solving the Einstein equation and relativistic hydrodynamic equations. Our formulation for solving them has been described in detail in [13, 14, 15, 8], so that we here briefly review the basic equations.

We write the line element in the form

$$ds^2 = g_{\mu\nu} dx^\mu dx^\nu = (-\alpha^2 + \beta_k \beta^k) dt^2 + 2\beta_i dx^i dt + \gamma_{ij} dx^i dx^j, \tag{1}$$

where $g_{\mu\nu}$, α, β^i ($\beta_i = \gamma_{ij}\beta^j$), and γ_{ij} are the 4D metric, lapse function, shift vector, and 3D spatial metric, respectively. Following previous papers [13, 14, 15, 8], we define the quantities to be solved in numerical computation as

$$\gamma = \det(\gamma_{ij}) \equiv e^{12\phi}, \tag{2}$$

$$\tilde{\gamma}_{ij} \equiv e^{-4\phi}\gamma_{ij} \ (\text{i.e., } \det(\tilde{\gamma}_{ij}) = 1), \tag{3}$$

$$\tilde{A}_{ij} \equiv e^{-4\phi}\left(K_{ij} - \frac{1}{3}\gamma_{ij} K_k{}^k\right), \tag{4}$$

where K_{ij} is the extrinsic curvature, and $K_k{}^k$ its trace. We note that indices of $\tilde{A}_{ij}$ and/or $\tilde{A}^{ij}$ are raised and lowered in terms of $\tilde{\gamma}_{ij}$ and $\tilde{\gamma}^{ij}$. In the numerical computation, we solve for $\tilde{\gamma}_{ij}$, $\tilde{A}_{ij}$, ϕ and $K_k{}^k$ instead of γ_{ij} and K_{ij}. Hereafter, we use D_i and $\tilde{D}_i$ as the covariant derivatives with respect to γ_{ij} and $\tilde{\gamma}_{ij}$, respectively.

As the matter source of the Einstein equation, we adopt a perfect fluid. In this case, the energy momentum tensor is written as

$$T_{\mu\nu} = (\rho + \rho\varepsilon + P) u_\mu u_\nu + P g_{\mu\nu}, \tag{5}$$

where ρ, ε, P, and u_μ are the rest mass density, specific internal energy density, pressure and four-velocity, respectively. Hereafter, we assume an equation of state of the form, $P = (\Gamma - 1)\rho\varepsilon$, where Γ is a constant and we adopt it in the range $1.8 \le \Gamma \le 2.5$ as a reasonable qualitative approximation to moderately stiff equations of state for neutron stars.

The hydrodynamic equations [continuity, Euler and energy (or entropy) equations] are written in the form

$$\partial_t \rho_* + \partial_i (\rho_* v^i) = 0, \tag{6}$$

$$\partial_t(\rho_*\hat{u}_k) + \partial_i(\rho_*\hat{u}_k v^i) = -\alpha e^{6\phi}\partial_k(P + P_{\rm art}) - \rho_*\Big[wh\partial_k\alpha - \hat{u}_j\partial_k\beta^j + \frac{\alpha e^{-4\phi}\hat{u}_i\hat{u}_j}{2wh}\partial_k\tilde{\gamma}^{ij} - \frac{2\alpha h(w^2-1)}{w}\partial_k\phi\Big], \quad (7)$$

$$\partial_t e_* + \partial_i(e_* v^i) = \dot{e}_{\rm art}, \quad (8)$$

where $\partial_\mu = \partial/\partial x^\mu$, $\rho_* = \rho w e^{6\phi}$, $h = 1 + \varepsilon + P/\rho$, $w = \alpha u^0$, $\hat{u}_k = hu_k$, $e_* = (\rho\varepsilon)^{1/\Gamma} w e^{6\phi}$, and

$$v^i \equiv \frac{u^i}{u^0} = -\beta^i + \frac{\alpha\tilde{\gamma}^{ij}\hat{u}_j}{whe^{4\phi}}. \quad (9)$$

$P_{\rm art}$ and $\dot{e}_{\rm art}$ denote the artificial viscosity [8]. In numerical simulation, we solve Eqs. (6)–(8) to evolve ρ_*, $\hat{u}_k$ and e_*.

Once $\hat{u}_i$ is obtained, $w(=\alpha u^0)$ is determined from the normalization relation of the four-velocity, which can be written as

$$w^2 = 1 + e^{-4\phi}\tilde{\gamma}^{ij}\hat{u}_i\hat{u}_j\left[1 + \frac{\Gamma e_*^\Gamma}{\rho_*(we^{6\phi})^{\Gamma-1}}\right]^{-2}. \quad (10)$$

The Einstein equation is split into the constraint and evolution equations. The Hamiltonian and momentum constraint equations are written in the form

$$R_k^{\ k} - \tilde{A}_{ij}\tilde{A}^{ij} + \frac{2}{3}(K_k^{\ k})^2 = 16\pi E, \quad (11)$$

$$D_i\tilde{A}^i_{\ j} - \frac{2}{3}D_j K_k^{\ k} = 8\pi J_j, \quad (12)$$

where $E \equiv T^{\mu\nu}n_\mu n_\nu$ and $J_i \equiv -T^{\mu\nu}n_\mu\gamma_{\nu i}$. $n_\mu = (-\alpha, 0)$ and R_{ij} denotes the Ricci tensor with respect to γ_{ij}.

Following [14, 15, 8], we write the evolution equations for the geometric variables in the form

$$(\partial_t - \beta^l\partial_l)\tilde{\gamma}_{ij} = -2\alpha\tilde{A}_{ij} + \tilde{\gamma}_{ik}\beta^k_{\ ,j} + \tilde{\gamma}_{jk}\beta^k_{\ ,i} - \frac{2}{3}\tilde{\gamma}_{ij}\beta^k_{\ ,k}, \quad (13)$$

$$(\partial_t - \beta^l\partial_l)\tilde{A}_{ij} = e^{-4\phi}\Big[\alpha\Big(R_{ij} - \frac{1}{3}e^{4\phi}\tilde{\gamma}_{ij}R_k^{\ k}\Big) - \Big(D_iD_j\alpha - \frac{1}{3}e^{4\phi}\tilde{\gamma}_{ij}D_kD^k\alpha\Big)\Big] + \alpha(K_k^{\ k}\tilde{A}_{ij} - 2\tilde{A}_{ik}\tilde{A}_j^{\ k}) + \beta^k_{\ ,i}\tilde{A}_{kj} + \beta^k_{\ ,j}\tilde{A}_{ki} - \frac{2}{3}\beta^k_{\ ,k}\tilde{A}_{ij} - 8\pi\alpha\Big(e^{-4\phi}S_{ij} - \frac{1}{3}\tilde{\gamma}_{ij}S_k^{\ k}\Big), \quad (14)$$

$$(\partial_t - \beta^l\partial_l)\phi = \frac{1}{6}\Big(-\alpha K_k^{\ k} + \beta^k_{\ ,k}\Big), \quad (15)$$

$$(\partial_t - \beta^l\partial_l)K_k^{\ k} = \alpha\Big[\tilde{A}_{ij}\tilde{A}^{ij} + \frac{1}{3}(K_k^{\ k})^2\Big] - D_kD^k\alpha + 4\pi\alpha(E + S_k^{\ k}), \quad (16)$$

where " $,i$ " denotes the partial derivative and $S_{ij} \equiv T^{\mu\nu}\gamma_{\mu i}\gamma_{\nu j}$.

In calculating R_{ij} and $R_k{}^k$ in Eq. (14), we have terms of the type as $\delta^{kl}\tilde{\gamma}_{ik,lj}$ and $\delta^{kl}\tilde{\gamma}_{jk,li}$. For evaluation of such terms and for stabilization of numerical system, we introduce the auxiliary variable $F_i = \delta^{jl}\partial_l\tilde{\gamma}_{ij}$ [14, 15] and solve the evolution equation

$$\begin{aligned}(\partial_t - \beta^l\partial_l)F_i &= -16\pi\alpha J_i + 2\alpha\Big\{ f^{kj}\tilde{A}_{ik,j} + f^{kj}{}_{,j}\tilde{A}_{ik} - \frac{1}{2}\tilde{A}^{jl}h_{lj,i} \\ &\qquad +6\phi_{,k}\tilde{A}^k{}_i - \frac{2}{3}(K_k{}^k)_{,i}\Big\} \\ &\quad -2\delta^{jk}\alpha_{,k}\tilde{A}_{ij} + \delta^{jl}\beta^k{}_{,l}h_{ij,k} + (\tilde{\gamma}_{il}\beta^l{}_{,j} + \tilde{\gamma}_{jl}\beta^l{}_{,i} - \frac{2}{3}\tilde{\gamma}_{ij}\beta^l{}_{,l})_{,k}\delta^{jk},\end{aligned} \tag{17}$$

where $h_{ij} = \tilde{\gamma}_{ij} - \delta_{ij}$, and $f^{ij} = \tilde{\gamma}^{ij} - \delta^{ij}$. Then, we evaluate $\delta^{kl}\tilde{\gamma}_{ik,lj}$ as $F_{i,j}$.

2.2 Gauge conditions

We adopt an approximate maximal slice (AMS) condition and an approximate minimum distortion (AMD) gauge condition as the time slicing and spatial gauge conditions, respectively [15, 8].

To impose the AMS condition, we solve the following parabolic type equation for $\ln\alpha$ at each timestep until an approximate convergence is achieved:

$$\begin{aligned}\partial_\lambda \ln\alpha &= D_kD^k\ln\alpha + (D_k\ln\alpha)(D^k\ln\alpha) - 4\pi(E + S_k{}^k) \\ &\quad - \tilde{A}_{ij}\tilde{A}^{ij} - \frac{1}{3}(K_k{}^k)^2 + f_\alpha K_k{}^k\rho_*^{1/2}.\end{aligned} \tag{18}$$

Here λ denotes a control parameter and f_α is a constant for which we assign a constant of $O(1)$. We note that in solving Eq. (18) at each time, we substitute a trial function of α which is extrapolated as $\alpha(x^i) = 2\alpha_{-1}(x^i) - \alpha_{-2}(x^i)$ where α_{-1} and α_{-2} denote the lapse function at previous two timesteps.

Assuming that the convergence is achieved and that the right-hand side of Eq. (18) becomes zero, the evolution equation for $K_k{}^k$ can be written as

$$(\partial_t - \beta^l\partial_l)K_k{}^k = -f_\alpha\alpha K_k{}^k\rho_*^{1/2}. \tag{19}$$

Thus, if $K_k{}^k$ is zero initially and the convergence is completely achieved, the maximal slicing condition $K_k{}^k = 0$ is preserved. Even when the convergence is incomplete and $K_k{}^k$ deviates from zero, the right-hand side of Eq. (19) enforces $|K_k{}^k|$ to approach to zero in the local dynamical timescale $\sim \rho_*^{-1/2}$. Hence, the condition $K_k{}^k = 0$ is expected to be satisfied approximately.

To impose the AMD gauge condition, we solve the following simple elliptic equations

$$\Delta P_i = S_i, \qquad \Delta\eta = -S_ix^i, \tag{20}$$

where Δ denotes the Laplacian in the flat 3D space, and

$$S_i \equiv 16\pi\alpha J_i + 2\tilde{A}_{ij}(\tilde{D}^j\alpha - 6\alpha\tilde{D}^j\phi) + \frac{4}{3}\alpha\tilde{D}_iK_k{}^k. \tag{21}$$

Equations for P_i and η are solved under the outer boundary conditions as

$$P_x = \frac{C_{xx}x}{r^3} + \frac{C_{xy}y}{r^3} + O(r^{-4}), \quad P_y = \frac{C_{yx}x}{r^3} + \frac{C_{yy}y}{r^3} + O(r^{-4}),$$
$$P_z = \frac{C_{zz}z}{r^3} + O(r^{-4}), \quad \eta = \frac{C_\eta}{r} + O(r^{-3}),$$

where $C_{xx}, C_{xy}, C_{yx}, C_{yy}, C_{zz}$, and C_η are constants which can be computed from the volume integration of $S_i x^j$ and $S_i x^i$.

From P_i and η, we determine β^i as

$$\beta^j = \delta^{ji}\left[\frac{7}{8}P_i - \frac{1}{8}(\eta_{,i} + P_{k,i}x^k)\right]. \tag{22}$$

Namely, β^i satisfies an elliptic type equation of the form

$$\delta_{ij}\Delta\beta^i + \frac{1}{3}\beta^k{}_{,kj} = S_j. \tag{23}$$

As we described in a previous paper [15], if an action

$$I = \int d^3x(\partial_t\tilde{\gamma}_{ij})(\partial_t\tilde{\gamma}_{kl})\tilde{\gamma}^{ik}\tilde{\gamma}^{jl}. \tag{24}$$

is minimized with respect to β^i, we obtain the equation of a minimum distortion (MD) gauge condition [16] for β^i as

$$\tilde{\gamma}_{jk}\tilde{D}^i\tilde{D}_i\beta^k + \frac{1}{3}\tilde{D}_j\tilde{D}_i\beta^i + \tilde{R}_{jk}\beta^k = S_j, \tag{25}$$

where $\tilde{R}_{jk}$ is the Ricci tensor with respect to $\tilde{\gamma}_{ij}$. Thus, the equation for β^i in the AMD gauge condition is obtained by neglecting coupling terms between β^i and h_{ij} in Eq. (25). Since the neglected terms are expected to be small [15], we can expect that I is approximately minimized in the AMD gauge condition.

The other benefit in the AMD gauge condition is that F_i is guaranteed to be small everywhere except in the strong field region just around a highly relativistic object [15]. This implies that a transverse condition, $\delta^{ij}\partial_i\tilde{\gamma}_{jk} = 0$, approximately holds for $\tilde{\gamma}_{ij}$ in the wave zone, helping the accurate extraction of gravitational waves near the outer boundaries of the computational domain.

One drawback of the AMD gauge condition together with the maximum slicing is that the resolution becomes quickly bad around high density region whenever the matter source collapses to be a black hole. To improve the resolution, we modify the AMD gauge condition using the same technique as that described in [15, 11, 9].

2.3 Initial value formalism

Even just before the merger, binary neutron stars are considered to be in a quasiequilibrium state because the timescale of gravitational radiation reaction $\sim 5/\{64\Omega$

$(M_g\Omega)^{5/3}\}$ [17], where M_g and Ω denote the total mass of the system and the orbital angular velocity of the binary neutron stars, is several times longer than the orbital period. Thus, for a realistic simulation of the merger, we should prepare a quasiequilibrium state as the initial condition. In this paper, we construct such initial conditions in the following manner.

First, we assume the existence of a helicoidal Killing vector, $\ell^\mu = (1, -y\Omega, x\Omega, 0)$. Since emission of gravitational waves violates the helicoidal symmetry, this assumption does not strictly hold in reality. However, as mentioned above, the emission timescale of gravitational waves is several times longer than the orbital period even just before the merger (*cf.* Table I) so that this assumption is acceptable for computing an approximate quasiequilibrium state.

In this paper, we consider binary neutron stars of irrotational velocity field. This assumption with the existence of the helicoidal Killing vector yields the hydrostatic equation

$$\frac{\alpha h}{w} + h u_k V^k = \text{const.}, \tag{26}$$

where $V^k = v^k - \ell^k$. Because of the irrotational velocity field, u_i is written as [18]

$$u_i = h^{-1}\partial_i \Phi, \tag{27}$$

where Φ denotes the velocity potential which satisfies an elliptic PDE [18]

$$\partial_i(\rho\alpha\psi^2 h^{-1}\tilde{\gamma}^{ij}\partial_j\Phi) - \partial_i[\rho\alpha h^{-1}\psi^6(\ell^i + \beta^i)] = 0. \tag{28}$$

The details of numerical methods for a solution of Φ are written in [19].

Initial conditions for geometric variables are obtained by solving the constraint equations (11) and (12), and equations for gauge conditions. Currently, we restrict our attention only to initial conditions in which $h_{ij} = 0 = \partial_t h_{ij}$ and $K_k{}^k = 0$.

Using the conformal factor $\psi \equiv e^\phi$, $\hat{A}_{ij} = \psi^6 \tilde{A}_{ij}$ and $\hat{A}^{ij} = \psi^6 \tilde{A}^{ij}$, the Hamiltonian and momentum constraint equations are rewritten in the form

$$\Delta\psi = -2\pi E\psi^5 - \frac{1}{8}\hat{A}_{ij}\hat{A}^{ij}\psi^{-7} \equiv S_\psi, \tag{29}$$

$$\hat{A}_i{}^j{}_{,j} = 8\pi J_i \psi^6. \tag{30}$$

After decomposition of $\hat{A}_{ij}$ in the standard manner [20] as

$$\hat{A}_{ij} = W_{i,j} + W_{j,i} - \frac{2}{3}\delta_{ij}\delta^{kl}W_{k,l}, \tag{31}$$

we set W_i as [14, 15]

$$W_i = \frac{7}{8}B_i - \frac{1}{8}(\chi_{,i} + B_{k,i}x^k), \tag{32}$$

where χ and B_i denote auxiliary functions. Then, Eq. (30) can be decomposed into two simple elliptic equations

$$\Delta B_i = 8\pi J_i \psi^6, \qquad \Delta\chi = -8\pi J_i x^i \psi^6. \tag{33}$$

Since $J_i\psi^6 (= \rho_* \hat{u}_i)$ is non-zero only in the strong field region, the solution of the momentum constraint equation is accurately obtained.

In addition to the constraint equations, we solve an elliptic type equation for α to impose $K_k{}^k = 0 = \partial_t K_k{}^k$ initially. In the conformally flat 3D space, the equation is written in the form

$$\Delta(\alpha\psi) = 2\pi\alpha\psi^5(E + 2S_k{}^k) + \frac{7}{8}\alpha\psi^{-7}\hat{A}_{ij}\hat{A}^{ij} \equiv S_{\alpha\psi}. \tag{34}$$

Equations for ψ, $\alpha\psi$, B_i and χ are solved under the outer boundary conditions as

$$\psi = \frac{C_\psi}{r} + O(r^{-3}), \quad \alpha\psi = \frac{C_{\alpha\psi}}{r} + O(r^{-3}), \quad B_x = \frac{C'_{xx}x}{r^3} + \frac{C'_{xy}y}{r^3} + O(r^{-4}),$$
$$B_y = \frac{C'_{yx}x}{r^3} + \frac{C'_{yy}y}{r^3} + O(r^{-4}), \quad B_z = \frac{C'_{zz}z}{r^3} + O(r^{-4}), \quad \chi = \frac{C_\chi}{r} + O(r^{-3}),$$

where $C_\psi, C_{\alpha\psi}, C'_{xx}, C'_{xy}, C'_{yx}, C'_{yy}, C'_{zz}$, and C_χ are constants which can be computed from the volume integration of S_ψ, $S_{\alpha\psi}$, $J_i x^j$ and $J_i x^i$.

We note that the elliptic equations for getting β^i [Eqs. (20)] are also solved at $t = 0$. If we construct $\tilde{A}_{ij}$ from β^i as

$$\tilde{A}_{ij} = \frac{1}{2\alpha}\left(\delta_{ik}\beta^k{}_{,j} + \delta_{jk}\beta^k{}_{,i} - \frac{2}{3}\delta_{ij}\beta^k{}_{,k}\right), \tag{35}$$

it satisfies the momentum constraint equation because $h_{ij} = 0$ at $t = 0$. Thus, $\tilde{A}_{ij}$ can be obtained either from Eq. (31) or from Eq. (35). The quasiequilibrium states which we use as the initial condition are obtained by solving equations for β^i instead of those for W^i [19], because we need to obtain β^i in solving hydrostatic equations.

In the following, we slightly reduce the angular momentum of quasiequilibriums at $t = 0$ to accelerate the merger. Whenever we add such perturbations, we recompute the equations of W^i and ψ for the perturbed values of ρ_* and u_i to guarantee that the constraint equations are satisfied at $t = 0$.

In the following, we often refer to the total rest mass, gravitational mass and angular momentum of the system at $t = 0$ which are calculated from

$$M_* = \int d^3x \rho_*, \tag{36}$$

$$M_g = \int d^3x \left(E\psi^5 + \frac{1}{16\pi\psi^7}\hat{A}_{ij}\hat{A}^{ij}\right), \tag{37}$$

$$J = \int d^3x (xJ_y - yJ_x)\psi^6. \tag{38}$$

We also refer to the relation between the rest mass and specific angular momentum which we define as

$$M_*(j) = \int_{j'>j} d^3x' \rho_*(x'), \tag{39}$$

Model	$(M/R)_\infty$	$\bar{\rho}_{\max}$	$\bar{M}_*$	$\bar{M}_g$	q	C_i	R_τ	$C_{\rm mass}$	L/M_g	Final product
(A)	0.12	0.139	0.186	0.173	1.03	0.090	5.1	0.58	37.5	neutron star
(B)	0.14	0.169	0.216	0.198	0.98	0.106	3.4	0.67	31.1	marginal
(C)	0.16	0.202	0.244	0.220	0.93	0.124	2.3	0.75	26.3	black hole

Table 1: A list of several quantities for initial conditions of irrotational binary neutron stars with $\Gamma = 2.25$. Compactness of each star in isolation $(M/R)_\infty$, the maximum density $\bar{\rho}_{\max} = K^n \rho_{\max}$, total rest mass $\bar{M}_* = K^{-n/2} M_*$, gravitational mass at $t = 0$ $\bar{M}_g = K^{-n/2} M_g$, $q = J/M_g^2$, a compactness $C_i \equiv (M_g\Omega)^{2/3} (\sim M_g/a$ where a is orbital separation), ratio of the emission timescale of gravitational waves to the orbital period $R_\tau = 5(M_g\Omega)^{-5/3}/128\pi$, the ratio of the rest mass of each star to the maximum allowed mass for a spherical star $C_{\rm mass} \equiv M_*/2M_{*\,\max}^{\rm sph}$, location of outer boundaries along each axis L/M_g and final products are shown. All quantities are normalized by K appropriately to be non-dimensional: We can rescale the mass to a desirable value by appropriately choosing K. Here, $M_{*\,\max}^{\rm sph}$ denotes the maximum allowed mass of a spherical star ($K^{-n/2} M_{*\,\max}^{\rm sph} \simeq 0.162$ at $K^n \rho_{\max} \simeq 0.52$).

where j denotes the specific angular momentum $j \equiv h u_\varphi$. $M_*(j)/M_*$ denotes rest mass fraction whose specific angular momentum is larger than a value j (i.e., $M_*(j=0)/M_* = 1$.)

2.4 Tests for code

Before carrying out simulations of the merger of binary neutron stars, it is necessary to confirm the accuracy and performance of our numerical code for many different problems. In particular, the following issues have to be addressed: (*i*) the merger will take place for a couple of orbital periods from the time when the binary just enters inside the innermost stable circular orbit to the formation of a black hole or neutron star. Can we carry out the simulation stably for such long timescale? (*ii*) the final product of the merger will either be a black hole or a neutron star. If the merged object is unstable against gravitational collapse, a black hole is formed. Can we judge the stability of the merged object against the gravitational collapse? (*iii*) the formation of a black hole will be signaled by the appearance of an apparent horizon. Can we determine the apparent horizon during the simulations? (*iv*) can we extract waveforms of gravitational waves?

To answer these questions, we have performed simulations for a wide variety of test problems such as (1) spherical collapse of dust ($P = 0$) to a black hole, (2) stability test of spherical stars in equilibrium, (3) excitation of quadrupole oscillations of perturbed spherical stars and emission of gravitational waves, (4) stability test of rapidly rotating stars in equilibrium, and (5) preservation of a corotating binary neutron star in a quasiequilibrium state. We presented the results in [8] and [9], which demonstrate that our numerical code can successfully perform such simulations.

3 Results

We have performed simulations for a wide range of Γ between 1.8 and 2.5. The results for $\Gamma = 2$ have already been presented in [11]. In this manuscript, we show

results for $\Gamma = 2.25$ which have recently been obtained. In Table 1, we list several quantities which characterize the quasiequilibrium state of irrotational binary neutron stars used in present simulations. All the quantities are non-dimensional appropriately scaled with respect to K. We also describe the final product in the last column. We choose binaries in the innermost orbits for which the Lagrange points appear at the inner edge of neutron stars [21]. Since the orbits of such binaries are stable, we reduce the angular momentum by $\sim 2\%$ (see discussion below). M_g and q listed in Table 1 are calculated from initial data sets which are recomputed after the reducing.

The simulations were performed using FACOM VPP 300/16R and VX/4R in the data processing center of National Astronomical Observatory of Japan (NAOJ). We have performed the simulations using a fixed uniform grid with the largest grid size $293 \times 293 \times 147$ for the $x-y-z$ directions, respectively, and assuming reflection symmetry with respect to the $z = 0$ plane. The grid covers the region $-L \le x, y \le L$ and $0 \le z \le L$ where L is a constant. The grid spacing is determined from the condition that major diameter of each star is covered with 35 grid points initially. With $293 \times 293 \times 147$ grid resolution, the computational memory required is about 20GBytes, and the computational time for one model is typically about 100 CPU hours for about 10000 timesteps. Test simulations have also been performed with $193 \times 193 \times 97$ grid resolution, to check the convergence of numerical results.

We should note that the wavelengths of gravitational waves should always be shorter than L, to accurately extract the waveform near the outer boundaries. However, taking such a large computation region is a very difficult task using present restricted computational resources. Since we need to adopt a grid spacing in which the diameter of each star is covered at least with ~ 30 grid points to avoid too large numerical dissipation and diffusion, the wavelength of gravitational waves for quasiequilibrium binaries at $t = 0$ is about three times longer than L in this work. This implies that gravitational waves in the early phase cannot be very accurately computed, although the wavelength of quasi-periodic waves of the merged object excited after merger (see Fig. 6) is much smaller than the wavelength of the binaries in quasiequilibrium and L so that the waveforms in the late phase can be computed fairly accurately. (See, e.g., [15] for numerical examples and discussion.)

As found in [21], orbits of all irrotational binaries with $\Gamma = 2.25$ are stable and the merger in reality should be triggered by radiation reaction of gravitational waves, which cannot be accurately computed here. To induce prompt merger by destabilizing the orbital motion, we initially reduce the angular momentum by $\sim 2\%$. More realistic simulation taking into account the radiation reaction in this early phase with a large computational region or with sophisticated wave extraction techniques [22] is a problem to be done in the future.

In Figs. 1 and 2, we display the density contour lines and velocity vectors for ρ_* and v^i at selected timesteps for simulations of models (A) and (C). For (A) the final product is a massive neutron star, and for (C) a black hole is formed and the apparent horizon was able to be located (thick solid circle in the last panel of

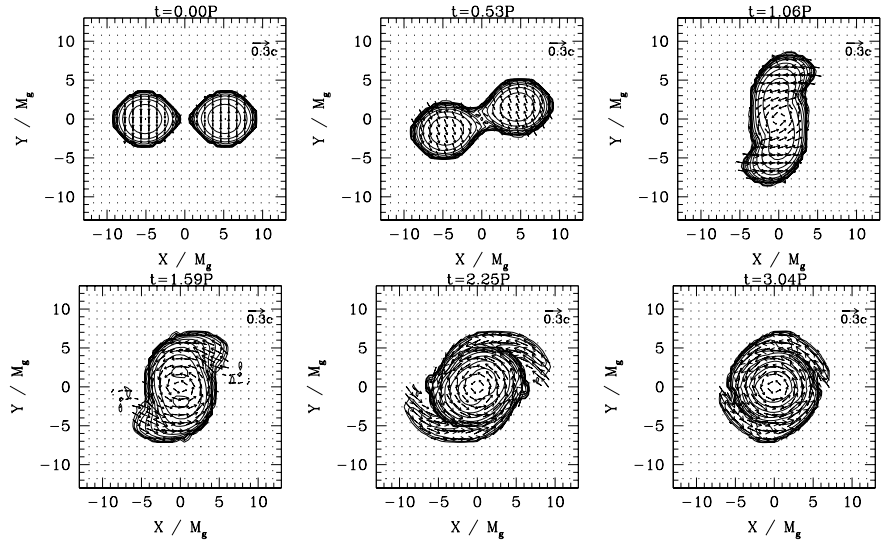

Figure 1: Snapshots of the density contours for ρ_* in the equatorial plane for model (A). The contour lines are drawn for $\rho_*/\rho_{*\,\max} = 10^{-0.3j}$, where $\rho_{*\,\max}$ denotes the maximum value of ρ_* at $t = 0$ (here $\bar{\rho}_{*\,\max} = 0.355$), for $j = 0, 1, 2, \cdots, 10$. The maximum density for ρ_* in the final panel is about 2.8 times larger than the initial value. Vectors indicate the local velocity field and the scale is as shown in the top left-hand frame. P denotes the orbital period of the initial quasiequilibrium. The length scale is shown in units of GM_g/c^2 where M_g is the gravitational mass at $t = 0$.

Fig. 2).

The rest mass of the binary for model (A) is $\sim 20\%$ larger than the maximum allowed value of a spherical star in isolation. Even with such large a mass, the merged object does not collapse to a black hole within a couple of dynamical timescales. As indicated in Figs. 1 and 2, the merging proceeds very mildly, because the approaching velocity at the contact of two stars is not very large. Consequently, the shock heating does not appear to be very important in merging. Indeed, the increase factor of P/ρ^Γ from initial value (i.e., K), which indicates the increase of the entropy, is quite small (at most 10%) around the central region of the merged object. This implies that the rotational centrifugal force plays an important role for supporting the self-gravity of such a large mass. To illustrate the importance of the rotation to support the large mass for model (A), the angular velocity along x and y axes and density contour lines in x-z slices for the merged object are displayed in Fig. 3. It is found that the merged object is differentially rotating, and the magnitude of the angular velocity is of order of the Kepler velocity, i.e., $\Omega M_g (R/M_g)^{3/2} = O(1)$. It is also found that the merged object has a highly flattened configuration as a result of this rapid rotation.

All these results are qualitatively the same as those found in the simulation for $\Gamma = 2$ [11]. However, the results are quantitatively different. In the case where $\Gamma = 2$, the maximum allowed rest mass for formation of the massive neutron star after merger is $\sim 1.5 M_{*\max}^{\rm sph}$ where $M_{*\max}^{\rm sph}$ denotes the maximum allowed rest mass

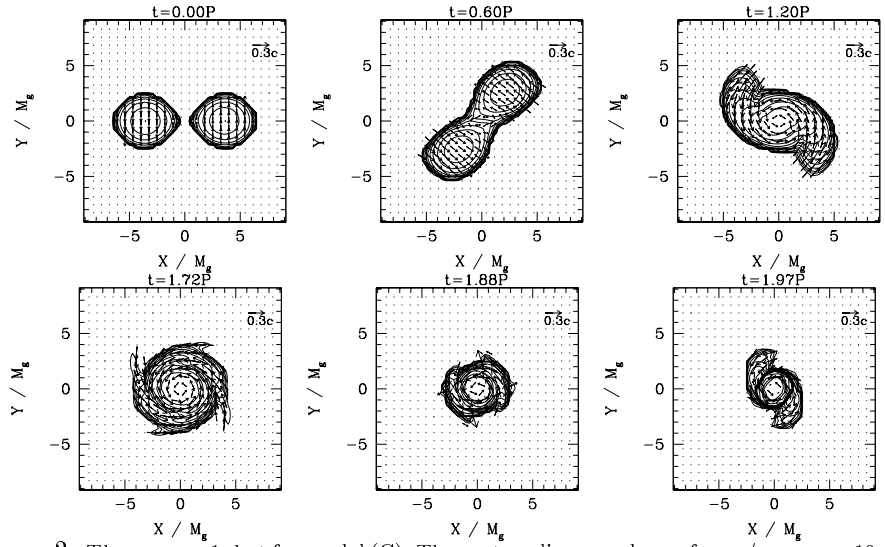

Figure 2: The same as 1, but for model (C). The contour lines are drawn for $\rho_*/\rho_{*\ \max} = 10^{-0.3j}$, where $\bar{\rho}_{*\ \max} = 0.757$, for $j = 0, 1, 2, \cdots, 10$. The maximum density for ρ_* in the final panel is about 80 times larger than the initial value. The thick solid circle in the final panel denotes the apparent horizon.

of a spherical star in isolation for a fixed value of Γ. As shown here, the threshold becomes $\sim 1.3 - 1.4 M^{\rm sph}_{*\rm max}$ for $\Gamma = 2.25$ (see below for discussion). We have also found that it is $\sim 1.6 - 1.7 M^{\rm sph}_{*\rm max}$ for $\Gamma = 1.8$. Thus, the threshold value depends sensitively on the stiffness of the equation of state.

For models (B) and (C) in which $(M/R)_\infty \geq 0.14$, a black hole is formed in our present simulations. However, the formation process is slightly different between models (B) and (C). For model (C), a black hole is quickly formed after the first contact of two neutron stars. On the other hand, the merger does not collapse quickly for model (B). In this case, the merged object quasi-radially oscillates for a couple of times after the first contact. Indeed, the lapse function at $r = 0$ does

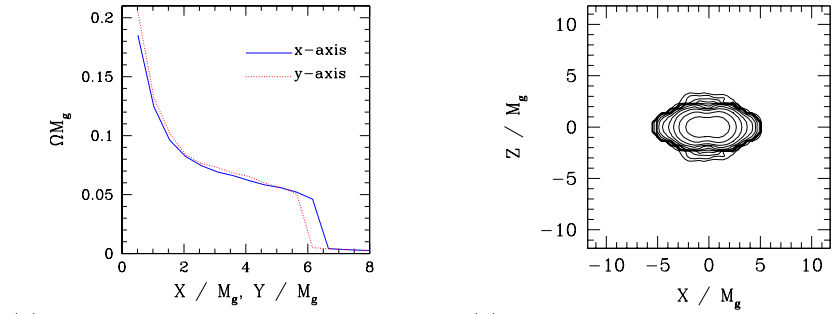

Figure 3: (a) The angular velocity in units of M_g^{-1} along x and y axes and (b) the density contour in x-z slices for the merged object of model (A). The contour lines are drawn in the same manner as for Fig. 1.

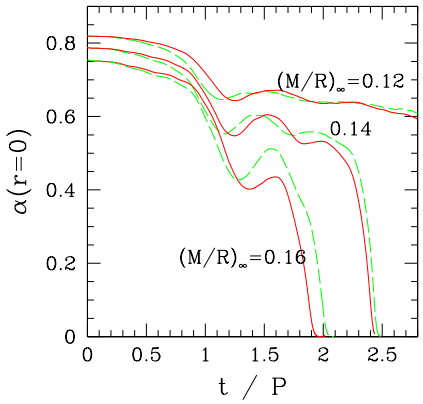

Figure 4: The lapse function α at $r = 0$ as a function of coordinate time for models (A)–(C). The solid and dashed lines denote the results for simulations with $293 \times 293 \times 147$ grid resolution and with $193 \times 193 \times 97$ grid resolution. For smaller scale simulations, the grid size is 116/96 times larger than that for larger scale simulations. (Namely, the outer boundaries along each axis are located $116L/146$ in these cases.)

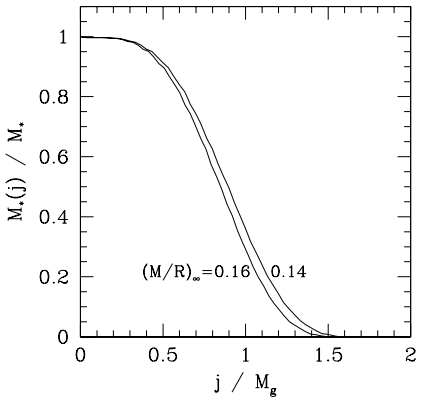

Figure 5: $M_*(j)/M_*$ as a function of j/M_g for quasiequilibrium configurations (B) and (C).

not quickly approach to 0 in this case, as shown in Fig. 4. The collapse toward a black hole seems to happen after dissipating angular momentum by gravitational radiation. As we will show below, the difference with regard to the formation process of black holes is reflected in the waveform of gravitational waves (see Fig. 6).

In Fig. 4, we also show the results for lower resolution simulations. It is found that convergence is achieved fairly well. However, with lower resolution, the numerical dissipation of the angular momentum is larger so that the merger happens earlier than that for higher resolution. Also, high density peaks are captured less accurately because of larger numerical diffusion. It is interesting to note that for even lower resolution, the merger for model (B) could avoid collapse, to be a massive neutron star because of large diffusion. Thus, we deduce that model (B) is near a threshold for the formation of a black hole. To determine the threshold of

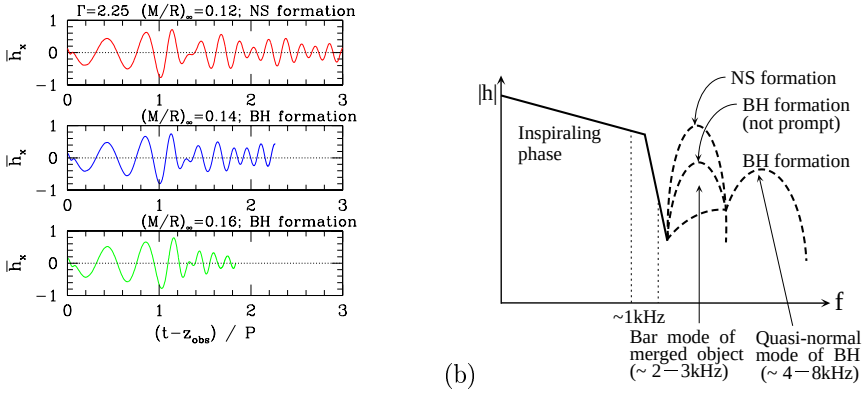

Figure 6: (a) $\bar{h}_\times \equiv \tilde{\gamma}_{xy}(r/M)(M/R)_\infty^{-1}$ near the outer boundary along the z-axis as a function of retarded time. (b) Schematic figure for the spectrum of gravitational waves. BH and NS denote black hole and neutron star, respectively. Frequency of quasi-normal modes is expected based on perturbation studies [23].

black hole formation more accurately, we need to perform more resolved numerical simulations in the future.

A noteworthy result for model (C) is that the rest mass outside the apparent horizon is less than 1% of the total mass. This implies that the fraction of rest mass in the disk around the black hole is very small. We note that for model (B), we were not able to determine the apparent horizon before the computation crashed. However, the mass fraction outside spheres of a fixed coordinate radius (e.g., $r = 1.5, 3$ and $4.5M_g$) is decreasing with time to be very small. Thus, we expect that the mass fraction of the disk is also very small in this case. In the following, we describe the reason for these results.

In Fig. 5, we show $M_*(j)$ at $t = 0$ as a function of j/M_g for models (B) and (C). It is found that there is no fluid element for which $j/M_g > 1.6$.

As we found in the simulations, a quite large fraction of the fluid elements are swallowed in the black hole. Gravitational radiation carries the energy from the system in particular in the early phase, but it should be less than 1% of M_g according to the quadrupole formula (see, e.g., [15]). Thus, the mass of the black holes is approximately equal to the initial value. On the other hand, the angular momentum may be dissipated by gravitational waves by about 10% of the initial value. These facts imply that $q = J/M_g^2$ should slightly decrease from the initial value to be $q \sim 0.9$ for both models. The specific angular momentum of a test particle in the innermost stable circular orbit around a Kerr black hole of mass M_g and $q = 0.9$ (0.95) is $\simeq 2.1M_g$ ($1.9M_g$). Therefore, *any fluid element of irrotational binary neutron stars just before the merger does not have enough specific angular momentum to form a disk around the formed black hole.* For the disk formation, some transport mechanism for angular momentum such as hydrodynamic interaction is necessary. Since the black holes are formed in the dynamical timescale of the system, the mechanism has to be very effective to transport the angular momentum by more than 30% in such short timescale. However, such a rapid process is unlikely

to happen as indicated in the present simulations.

In Fig. 6 (a), we show

$$\bar{h}_\times \equiv \tilde{\gamma}_{xy}\left(\frac{r}{M_g}\right)\left(\frac{M}{R}\right)^{-1}_{\infty}, \tag{40}$$

as a function of retarded time along the z-axis near the outer boundary as a measure of $\times$-mode gravitational waves. We should note again that the outer boundaries along each axis reside inside the wave zone (i.e., $L \sim \lambda_{\rm gw}/3$, where $\lambda_{\rm gw}$ denotes the characteristic wavelength of gravitational waves) in the early stage of the simulation, so that the wave amplitude for $t - z_{\rm obs} \lesssim P$ is not very accurate. We should take into account an error of $O(10\%)$. However, for $t - z_{\rm obs} \gtrsim P$, L is less than $\lambda_{\rm gw}$ because the characteristic wavelength becomes short after the merger starts. Therefore, we can consider that the waveforms in the late phase are fairly accurate.

In the case when a massive neutron star is formed, quasi-periodic gravitational waves of a fairly large amplitude, which are excited due to the non-axisymmetric deformation and oscillation of the merged object, are emitted even after the merger. Since the radiation reaction timescale is much longer than the dynamical (rotational) timescale of the massive neutron star, the quasi-periodic waves will be emitted for many rotational cycles.

Even for the case of black hole formation, quasi-periodic gravitational waves are excited due to the non-axisymmetric oscillation of merged objects before collapse. Since the computation unfortunately crashed soon after the formation of the apparent horizon, we cannot draw a definite conclusion from our simulation with regard to gravitational waves in the last phase. However, we can expect that after the formation of the black holes, quasi-normal modes of the black holes are excited and gravitational waves will damp eventually. Since the formation timescale of the black holes is different between models (B) and (C) depending on initial compactness of neutron stars, duration of the quasi-periodic waves induced by non-axisymmetric oscillations of the merged objects is also different. From these results, the spectrum of gravitational waves after the merging phase may be illustrated as in Fig. 6 (b). The frequency of the quasi-periodic oscillation is about 5 or 6 times higher than the orbital angular frequency of quasiequilibrium binaries at $t = 0$, and thus,

$$f \sim 2{\rm kHz}\left(\frac{2.8M_\odot}{M_g}\right)\left(\frac{C_i}{0.1}\right)^{3/2}. \tag{41}$$

As we explained above, the amplitude of the Fourier peak for the quasi-periodic oscillation is determined by the duration of the quasi-periodic oscillation and hence, depends strongly on the initial compactness of neutron stars and final product. Therefore, by observing the amplitude of this peak, we will be able to obtain information for compactness of neutron stars before the merger and the final product. From gravitational waves emitted in the inspiraling phase with post Newtonian template of waveforms [24], mass of two neutron stars, and hence, total mass will be determined [25]. This also implies that from the amplitude of the quasi-periodic

oscillation emitted by the merged object, we could also constrain the maximum allowed mass of neutron stars, and, therefore, nuclear equations of state.

Since the frequency of this peak is rather high, it is difficult to detect by first generation, kilo-meter-size laser interferometers such as LIGO I and VIRGO. However, the resonant-mass detectors and/or specially designed narrow band interferometers may be available in future, to detect such high frequency gravitational waves. These detectors will provide us a wide variety of information on neutron star physics.

4 Summary

We have performed fully GR simulations of merging neutron stars. As demonstrated in this manuscript, the simulations are feasible to yield scientific results stably and fairly accurately.

One of the most interesting results found in this work is that the products after merger depend sensitively on the compactness of neutron stars before merger. If the total rest mass of the system is sufficiently (1.3–1.7 times depending on Γ) larger than the maximum rest mass of a spherical star in isolation, a black hole is formed, and otherwise, a massive neutron star is formed. It is noteworthy that the rest mass of the massive neutron star can be significantly larger than the maximum value for a spherical star of identical equation of state. The self-gravity of such high mass neutron stars can be supported by a rapid, differential rotation [11, 10]. We also found that the difference of the final products is significantly reflected in the waveforms of gravitational waves, suggesting that detection of gravitational waves of high frequency could constrain the maximum allowed mass of neutron stars.

In the case of prompt black hole formation, the disk mass is found to be very small, i.e., less than 1% of the total rest mass. The main reason is that the specific angular momentum of all the fluid elements in binary neutron stars of irrotational velocity field just before the merger is too small and transport timescale of the angular momentum is not short enough to help the disk formation. It should be noted that this conclusion may hold only for binary neutron stars of nearly equal mass. In binaries of unequal mass, the conclusion could be modified, because the neutron star of smaller mass may be tidally disrupted before the separation of two stars becomes very small and hence, before the angular momentum of the system is not significantly dissipated by gravitational radiation. In this case, many of the fluid elements in the neutron star of smaller mass may have large enough angular momentum to form a disk during the merger. To clarify whether such scenario is promising or not, it is necessary to perform simulations for merger of binary neutron stars of unequal mass.

Finally, we point out the problem to be resolved and discuss the prospect for the near future. As we mentioned in Sec. 3, the computational domain is not so large that the outer boundaries are resided inside the wavelength of gravitational waves emitted by binary neutron stars in the early phase of merger. To overcome this problem, it may be necessary to install sophisticated matching techniques for the wave zone [22], if computational resources are still restricted. From January

2001, however, we will be able to use more powerful supercomputers in NAOJ, which have a memory of about several hundred GBytes. With such machines, the outer-boundary problem may be improved significantly.

Acknowledgments

The author would like to thank D. Sciama, J. Miller and L. Rezzolla for inviting him to this meeting and giving him the opportunity to present the results of recent efforts. This work is partly carried out in collaboration with K. Uryu, to whom the author would like to express his thanks. He also thanks T. Baumgarte, E. Gourgoulhon, J. Miller, T. Nakamura, K. Oohara, L. Rezzolla and S. Shapiro for helpful discussions and comments, and the Department of Physics of the University of Illinois, where most of this work was carried out, for warm hospitality. Numerical computations were performed on the FACOM VPP 300/16R and VX/4R machines in the data processing center of NAOJ. This work was supported by JSPS (Fellowships for Research Abroad).

References

[1] For example, K. S. Thorne, in *Proceedings of Snowmass 95 Summer Study on Particle and Nuclear Astrophysics and Cosmology*, eds. E. W. Kolb and R. Peccei (World Scientific, Singapore, 1995), p. 398, and references therein.

[2] E. S. Phinney, Astrophys. J. **380**, L17 (1991): R. Narayan, T. Piran and A. Shemi, Astrophys. J. **379**, L17 (1991).

[3] For example, R. Narayan, B. Paczynski, and T. Piran, Astrophys. J. **395**, L83 (1992):
M. J. Rees, in *Proceedings of the Eighteenth Texas Symposium on Relativistic Astrophysics, and Cosmology*, eds. A. V. Olinto, J. A. Frieman, and D. N. Schramm (World Scientific, 1998), p. 34: H.-Th. Janka and M. Ruffert, Astron. Astrophys. **307**, L33 (1996): P. Meszaros, astro-ph/9904038.

[4] M. R. Metzger et al., Nature **387**, 878 (1997): S. R. Kulkarni et al., Nature **393**, 35 (1998).

[5] K. Oohara, T. Nakamura, and M. Shibata, Prog. Theor. Phys. Suppl. **128**, 183 (1997) for a review before 1997: For recent researches, e.g., J. A. Faber and F. A. Rasio, Phys. Rev. D **62**, 064012 (2000).

[6] K. Oohara and T. Nakamura, Prog. Theor. Phys. Suppl. **136**, 270 (1999).

[7] J. A. Font, M. Miller, W.-M. Suen, and M. Tobias, Phys. Rev. D **61**, 044011 (2000).

[8] M. Shibata, Phys. Rev. D **60**, 104502 (1999).

[9] M. Shibata, T. W. Baumgrate, and S. L. Shapiro, Phys. Rev. D **61**, 044012 (2000).

[10] T. W. Baumgrate, S. L. Shapiro, and M. Shibata, Astrophys. J. Lett. **528**, L29 (2000).

[11] M. Shibata and K. Uryu, Phys. Rev. D **61**, 064001 (2000).

[12] M. Shibata, T. W. Baumgrate, and S. L. Shapiro, Astrophys. J. **542** (2000) in press.

[13] M. Shibata and T. Nakamura, Phys. Rev. D **52**, 5428 (1995).

[14] M. Shibata, Prog. Theor. Phys. **100**, 251 (1999).

[15] M. Shibata, Prog. Theor. Phys. **101**, 1199 (1999).

[16] L. Smarr and J. W. York, Phys. Rev. D **17**, 1945 (1978): Note that the definition of the minimum distortion gauge in this paper is slightly different from the original version by Smarr and York.

[17] S. L. Shapiro and S. A. Teukolsky, *Black Holes, White Dwarfs, and Neutron Stars*, Wiley Interscience (New York, 1983).

[18] M. Shibata, Phys. Rev. D **58**, 024012 (1998): S. A. Teukolsky, Astrophys. J. **504**, 442 (1998): See also, S. Bonazzola, E. Gourgoulhon and J.-A. Marck, Phys. Rev. D **56**, 7740 (1997): H. Asada, Phys. Rev. D **57**, 7292 (1998).

[19] K. Uryu and Y. Eriguchi, Phys. Rev. D **61**, 124023 (2000): See also, E. Gourgoulhon et al., gr-qc/0007028.

[20] J. W. York, Jr., in *Sources of Gravitational Radiation*, ed. L. L. Smarr (Cambridge University Press, 1979), 83.

[21] K. Uryu, M. Shibata and Y. Eriguchi, Phys. Rev. D (2000), to be published: See also, K. Uryu, this volume.

[22] N. Bishop et al., Phys. Rev. Lett. **76**, 4303 (1996): A. M. Abrahams et al., Phys. Rev. Lett. **80**, 1812 (1998): L. Rezzolla et al., Phys. Rev. D **59**, 064001 (1999).

[23] E. W. Leaver, Proc. R. Soc. London **A402**, 285 (1985).

[24] L. Blanchet, B. R. Iyer, C. M. Will and A. G. Wiseman, Class. Quant. Grav. **13**, 575 (1996).

[25] C. Cutler and E. E. Flanagan, Phys. Rev. D **49**, 2658 (1994): E. Poisson and C. M. Will, *ibid* **52**, 848 (1995).